Moment-resisting self-drilling dowel connections between steel link beams and CLT for coupled walls

Ben Moerman[1*], Minghao Li[1], Alessandro Palermo[1], and Angela Liu[2]

[1]Department of Civil and Natural Resources Engineering, University of Canterbury, Christchurch, New Zealand

[2]BRANZ, Wellington, New Zealand

*Corresponding Author

Abstract

Coupled cross-laminated timber (CLT) walls can be created by connecting steel link beams between adjacent CLT wall panels and present an efficient alternative to conventional cantilevered CLT shear walls. Effective coupling in the coupled wall system requires the beam to wall connections to have adequate strength to ensure a ductile link beam response and adequate stiffness to yield the link beams at relatively low inter-storey drifts. This study evaluates beam to wall connections with a group of self-drilling dowels (SDDs) installed through a steel knife plate to connect 200UB18 steel link beams to 5-ply CLT walls. A method for determining the connection strength is presented within a capacity design framework and compared to the results of the three experimental tests. The capacity design method was validated for the tested specimens because the damage was concentrated in the steel link beams and the connection's peak strength was not exceeded. This study indicates that the SDD connections may be a feasible beam to wall connection solution in the proposed coupled CLT wall system because the capacity protected connections had adequate strength and relatively high stiffness.

Keywords: Cross laminated timber, coupled walls, timber connections, self-drilling dowels

1. Introduction

Mass timber buildings using cross laminated timber (CLT) have been gaining global popularity over the last decade in part due to reduced cost of mass timber products and sustainability considerations by building owners. For the seismic design of mid and high-rise CLT buildings, coupled walls offer unique advantages as a lateral load resisting system as they can provide flexibility for fitting within architectural plans and enhanced strength, stiffness, and system ductility when compared with single cantilevered shear walls. One type of coupled mass timber wall system with steel link beams was first introduced by Karsh and Green [1] in the FFTT *(Finding the Forest Through the Trees)* building system. The FFTT system proposed the use of a timber core assembly using solid wood panels with embedded steel beams to provide coupling and optional perimeter steel moment frames to form a dual system for taller buildings. This coupled wall system was investigated by Zhang et al. [2] at the system level by running nonlinear time history analyses to estimate appropriate seismic design factors for the use within the Canadian National Building Code [3]. In addition, a further study by Zhang et al. [4] using more complex reliability analyses demonstrated that the proposed seismic design factors were appropriate. Link beam connection testing was undertaken by Bhat [5] and Azim [6] and was used to calibrate the nonlinear models used by Zhang et al. [2] in the previously mentioned studies (see summary by Zhang et al. [7]).

The link beam-to-wall connection proposed in the FFTT system consisted of a horizontal notch in the CLT wall panel where the steel beam was embedded to transfer the loads through steel-to-timber bearing at its top and bottom flange surfaces. The experiments by Bhat [5] and Azim [6] demonstrated its ability to provide adequate strength to achieve ductile responses of the link beams but the damage was not always limited to the link beams. The eccentric configuration between the link beam and CLT wall caused wood splitting and rolling shear failures in the experiments which either prevented the steel beam from reaching its peak strength or caused significant pinching of the hysteretic loops under cyclic loads. Additionally, the FFTT connection requires a significant amount of wood removed from the CLT wall to create the notch for beam embedment, which may cause design issues due to the reduced net cross sections over the height of the CLT walls. Therefore, alternative connection types between steel beams and solid timber walls, like the one in this study, may provide engineers with attractive alternatives to create coupled CLT wall systems.

A simplified diagram of a coupled CLT wall system with steel link beams is shown in Figure 1. The link beam connections transfer shear and bending loads between the beam and wall elements and significantly affect the system performance in an earthquake. Adequate stiffness and tightness must be provided by the connections to ensure the link beams are engaged at relatively low drift levels. In addition, they should be protected from severe damage in major earthquakes as the steel link beams are designated as ductile elements responsible for dissipating energy.

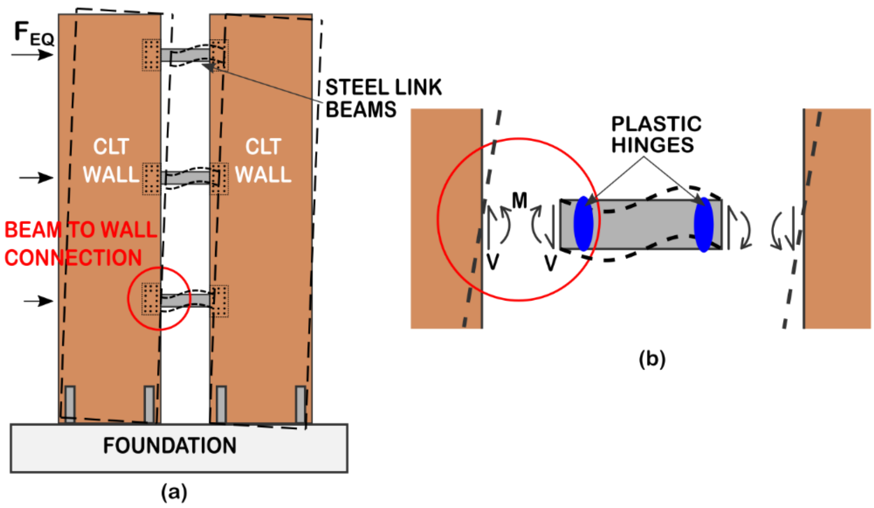

Figure 1: Coupled CLT wall structure behaviour under earthquake loading with beam to wall connection highlighted (a) and deformed shape with connection forces under lateral loading (b).

Small fasteners like nails and timber rivets can be used to create moment connections between timber beams and columns, such as the knee joints in timber portal frame structures [8]. However, they are not applicable for the beam to wall connections in the coupled CLT wall system because many fasteners are required to transfer significant loads. Conventional dowels or bolts are often used for large capacity timber connections because they are simple and economical [9]. However, timber splitting often limits the moment capacity of these connections due to high perpendicular to grain tensile stresses in the connection and reinforcing methods are needed. Self-tapping screws can be used for reinforcing timber perpendicular to grain, as demonstrated by Lam et al. [10]. In addition to potential splitting, a concern for bolts is the oversized holes (typically 1-2mm larger than the bolt diameter) are required for assembly. The oversized holes may cause initial slips of the connections and significantly delay engagement of the steel link beams in the coupled wall system until large interstorey drifts are experienced by the structure.

An experimental study by Dong et al. [11] demonstrated the ability to create strong, stiff, and tight moment connections for glulam beam-column joints using self-drilling dowels (SDDs). The SDD connections do not require predrilling in timber and can be drilled through internal steel knife plates with a high-speed drill up to a certain thickness. The glulam members used self-tapping screw reinforcement to prevent premature timber splitting. In contrast to glulam, CLT is not as susceptible to splitting failures due to its orthogonal layup [12] and therefore screw reinforcement may not be required. The authors also presented an analytical method for predicting the monotonic behaviour of the SDD moment connections which agreed well with the test results.

SDDs may also have the potential to create moment connections between steel link beams and CLT walls in a coupled timber wall system. Commonly available Ø7mm SDDs (Figure 2c) have a drilling tip to create their own holes through timber and internal steel plates, which creates a tight connection. Additionally, a threaded region under the head creates additional forces to pull dowels into the timber. An SDD group connection's strength depends on: (1) the amount and diameter of dowels, (2) group spacing and edge distances, (3) the number of internal plates (i.e. amount of shear planes), and (4) the strength and thickness of the timber.

In this study, a type of SDD connection, shown in Figure 2, is proposed to connect the steel link beams in coupled CLT wall systems. The link beam is welded to an end plate which is welded to a knife plate. The knife plate is inserted into a slot in the CLT panel's edge and SDDs are then installed through the CLT panel and the knife plate to connect the assembly together. This study presents analytical predictions and experimental testing of this connection type to evaluate the feasibility and robustness of the SDD connections.

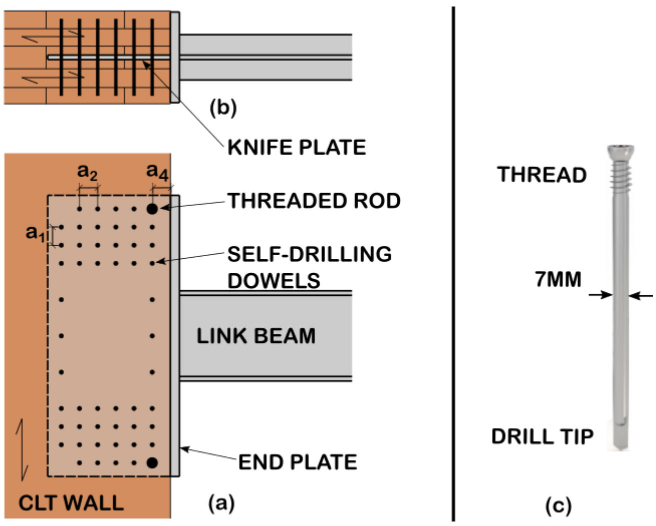

Figure 2: Typical self-drilling dowel group beam to CLT wall connection (a, b) and typical self-drilling dowel fastener (c).

2. SDD Connection Design

2.1. Analytical method

The strength of SDD moment connections can be calculated using an iterative approach based on the analytical method presented by Dong et al. [11]. Their study found the method to be a conservative prediction of their experimental results and was more accurate than the other three analytical methods proposed for the glulam specimens in their study. However, the complexity of the analytical method is likely too rigorous for routine use by practicing engineers. Therefore, two simplifying modifications were made to the Dong et al. method in this study to reduce the complexity: (1) the bearing stresses between the beam and the column were assumed to have a triangular stress block with the peak stress of $f_{c,0}$ and (2) the centre of rotation was not restricted to an assumed trajectory. This simplified method can be more readily implemented in a spreadsheet for design applications.

It is expedient to only consider two strength levels when analysing the connection: the yield ($M_{c,y}$ and V_y) and ultimate ($M_{c,u}$ and V_u) strengths; which can be found by determining the force at which the first dowel yields and all the dowels yield, respectively. This method assumes that all the dowels can achieve an adequate level of ductility to deform beyond their yield displacement and presumes simple elastic-plastic behaviour of each SDD (no strain hardening). Alternatively, a complete backbone moment-rotation plot may also be found by evaluating the forces for the progressive yielding of the dowel group. This approach is used and compared to the experimental results in Section 4.2.

Figure 3 shows the forces and notations used to determine the connection strength. Applied forces are shown in blue while the resisting forces are shown in red. The applied moment is shown at 3 locations: M at the end of the link beam, M_c at the geometric centroid of the dowel group, and M'_c at the centre of rotation. M'_c, shown at the centre of rotation (O'), is relevant for calculating the connection strength because it is about point O' that the moments are summed and is related to the moment at the geometric centroid by $M'_c = M_c + x'_o V$.

The solution process and governing equilibrium equations are summarized below but further detail is available in Dong et al [11]. First, a single dowel's nominal strength, F_d, is calculated using the Johansen equations [13,14] which are used in Eurocode 5 [15]. Second, a centre of rotation (O') is assumed, shown in Figure 3, and the individual dowel forces are determined. The individual SDD forces vary based on whether the connection yield (V_y) or ultimate strength (V_u) is being determined. The yield strength of the connection is found by assuming SDD forces are proportional to their relative distance from the centre of rotation ($f_i = F_d r'_i / r'_{max}$), where the dowel furthest from point O' has a force equal to its yield strength. Alternatively, the ultimate connection strength assumes all SDDs have yielded ($f_i = F_d$).

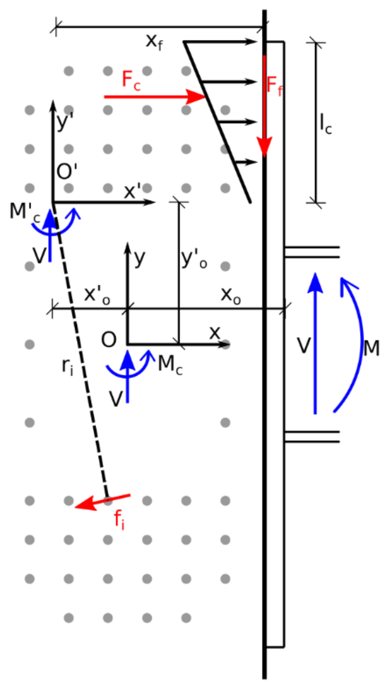

Figure 3: Free body diagram and notation for calculating dowel group connection strength (applied forces in blue, resisting forces in red).

Third, the equilibrium of the connection is checked, using the assumed centre of rotation (O'), with the following governing equations:

$$\sum F_x = F_c + \sum f_{x,i} = \frac{l_c b_{ef} f_{c,0}}{2} + \sum f_{x,i} = 0 \tag{1}$$

$$\sum F_y = -\sum f_{y,i} - F_f + V = -\sum f_{y,i} - \mu \frac{l_c b_{ef} f_{c,0}}{2} + V = 0 \tag{2}$$

$$\sum M = \sum f_i r_i + \frac{2l_c}{3} F_c + F_f x_f - M'_c = 0 \tag{3}$$

where

F_c is the contact force,

l_c is the contact length,

b_{ef} is the total CLT board thickness oriented parallel to the F_c,

$f_{c,0}$ is the compression strength of the boards oriented parallel to F_c,

$f_{x,i}$ and $f_{y,i}$ are the SDD component forces,

F_f is the friction force (μF_c),

μ is the friction coefficient (0.2 for steel-timber contact),

and other dimensions are as shown in Figure 3.

If these equilibrium equations are not satisfied within an acceptable error tolerance, then a new centre of rotation must be assumed and the terms are recalculated until an acceptable level of accuracy is achieved.

2.2. Connection Stiffness

The connection's pre-yield rotational stiffness can be estimated by evaluating the rotation at which the first SDD yields. The individual dowel stiffness $k_{sdd} = \rho^{1.5}d/23$ in Eurocode 5 [15] can be used unless specific test data is available. The following equation is used to determine an approximate rotational stiffness for the connection:

$$k_{rot} = \frac{M'_{c,y}}{\arctan\left(F_d/\left(k_{sdd} r_{max}\right)\right)} \tag{4}$$

where $M'_{c,y}$, F_d, and r are defined in Section 2.1.

In addition, the pre-yield translational stiffness of the connection can be approximated by the number of SDDs multiplied by the individual dowel stiffness ($k_v = nk_{sdd}$).

2.3. Capacity Design

A coupled timber wall system should yield the steel link beams to dissipate energy during major earthquakes and capacity design should be used to prevent premature failures in non-dissipative elements [16,17]. The capacity design process includes multiplying the link beam's nominal strength ($V_{b,n}$) by an overstrength factor (ϕ_o) to determine an amplified force demand on the non-dissipative connection or element. In a simplified form, the link beam's overstrength can be determined as the overstrength factor multiplied by the minimum of its nominal shear or bending strength:

$$V_{b,os} = \phi_o V_{b,n} = \phi_o MIN\left(0.6F_y A_w, 2F_y Z/e\right) \tag{5}$$

where F_y is the specified minimum yield stress, A_w is the web area, Z is the plastic section modulus, and e is the link beam length.

However, eccentric braced frame (EBF) link beam design requirements in relevant design standards should be followed for calculating the link beam strength in a coupled wall structure to consider the additional factors such as (but not limited to) axial force interactions, deformation capacity as a function of link length [18], and web stiffener requirements.

Overstrength factors will vary based on the specified grade of steel and the applicable national design standard. The New Zealand steel standard (NZS 3404 [19]) provides an overstrength factor of 1.67 for hot rolled steel sections produced in accordance with the AS/NZS 3679.1 standard [20]. A notably lower factor of 1.21 is found in the American steel standard (AISC 341 [21]) for A992 steel sections because this grade has an upper bound on the yield stress. Therefore, engineers can design a more economical structure by using steel grades with lower overstrength.

The specimens in this study used a 200UB18 section with an effective link length of e=760mm (twice the cantilever length in the test setup) and specified minimum yield stress of F_y=300MPa. The nominal link beam strength and overstrength were determined using Equation **Error! Reference source not found.** as $V_{b,n}$=142kN and $V_{b,os}$=237kN. Therefore, the overstrength force demand on the dowel group was calculated as V=237kN and M_c=128kNm.

Using the analytical method described in Section 2.1, the connection’s nominal yield and ultimate strengths (i.e. material strength reduction factor of 1.0) were found to be V_y=177kN and V_u=239kN, respectively. The nominal connection strength was calculated with a characteristic board compression strength of $f_{c,0}$=18Mpa and a single Ø7x170mm SDD nominal strength of F_d=11.2kN. The nominal SDD strength was found using the European Yield Model equations from Eurocode 5 (EC5) [15] with a characteristic embedment strength of f_h=32MPa (characteristic prediction from Uibel and Blaß [22]) and yield moment of m_y=32,000Nmm [23]. It should be noted that a modified version of Equation 8.11 (h) in EC5 was used, shown in Equation (6) without the rope effect term, to determine the nominal dowel strength because the pre-factor of 2.3 is used to adjust the equation for a material safety factor of $\gamma_{M,steel}$=1.3 (see discussion in Blaβ and Sandhaas [14]). No modification factor was used because CLT is not explicitly addressed in EC5 Table 3.1 (i.e. k_{mod}=1), although a factor of 1.1 may be justified.

$$2.0\sqrt{M_{y,Rk}f_{h,1,k}d} \tag{6}$$

The ultimate nominal connection strength is greater than the link beam's overstrength demand (V_u 239kN > $V_{b,os}$ 237kN) but the connection's yield strength is lower. Therefore, some yielding of the SDDs is implicitly accepted in the test specimen. It may or may not be acceptable, within the goals of a performance-based design framework, to allow yielding of the dowels in a DG connection.

In addition to specifying the amount, size, and spacing of the fasteners, the designer must also ensure the other non-ductile components including the welds, end plate, and knife plate along the load path are stronger than the link beam's overstrength demand. Also, the CLT wall panel's shear and bending strength would need to be greater than the cumulative effect of the coupling beams' overstrength demands. These components are just as important as the SDD group but detailed design of the other elements is beyond the scope of this study.

3. Experiment Details and Setup

3.1. Specimen details and material properties

Three identical specimens were fabricated and tested until failure, including one monotonic test (DG10-M) and two cyclic tests (DG11-C, DG12-C). Each specimen consisted of an SDD group connection with 50-Ø7x170mm between a 200UB18 steel link beam and a 205mm (45/35/45/35/45) CLT wall panel, shown in Figure 4. Typical minimum spacing and edge distances of a_1=a_2=a_4=40mm were used. The edge distance (a_2) was below the minimum required value from the product specification (80mm) [23] for sawn timber but no limit is specified for CLT. The limit for sawn timber was ignored because the orthogonal layup of CLT reduces the tendency for edge splitting. Two M20 threaded rods with nuts and washers were also installed at the extremes of the dowel group near the CLT edge. This was done according to the recommendations from Blaß and Sandhaas [18] to prevent timber from splitting (prying open) in the thickness of the timber member. The threaded rods were not considered when calculating the connection strength because of the oversized hole diameters (2mm greater than rod diameter) used to install these rods.

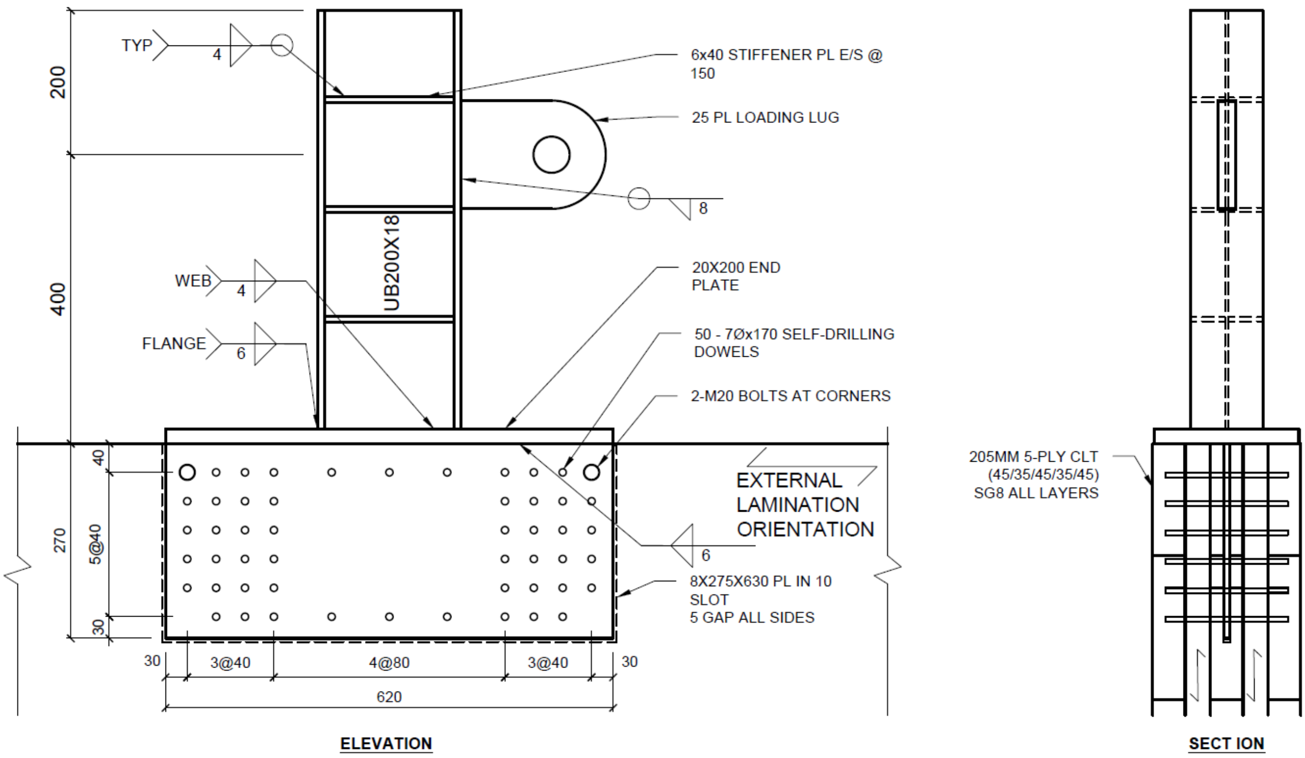

Figure 4: Self-drilling dowel group connection and link beam specimen details.

SDDs were concentrated near the extreme edges of the knife plate as this maximised the moment strength. The 200UB18 link beam was welded to a 20mm-thick steel end plate which was welded to an 8mm-thick knife plate. A typical 6mm fillet weld was used except at the beam's web where a 4mm fillet weld was specified. 6mm plate stiffeners were welded on both sides of the web at 150mm centres which meets the requirements of an active EBF link according to the NZ Steel Design Standard NZS3404 [19].

Ø6x25mm pilot holes were pre-drilled on the timber surface to prevent surface splitting and the SDD were installed using a high-speed drill according to the manufacturer's specifications [23]. All experiments used 5-ply CLT wall panels (45/35/45/35/45) with the face layers oriented perpendicular to the link beam's axis. The CLT was made of 45mmx200mm primary boards (grade SG8 [24]) and 35mmx175mm cross layers (grade SG6) Radiata Pine with a mean density of 460kg/m^3 and COV of 0.042. The mean moisture content, measured by oven-dried samples, was 11% at the time of testing and the COV was 0.045. The characteristic compressive strength $f_{c,0}$=18MPa for the SG8 boards was used to calculate the connection's nominal strength in Section 2.3. The steel link beams in the ductile tests were fabricated from standard hot rolled I-beam sections (Grade 300) in accordance with AS/NZS 3679.1-300SO [20].

3.2. Experiment setup and instrumentation

For testing convenience, the connection specimens were rotated 90 degrees from their real orientation in a coupled wall system. The panel was anchored to the concrete strong floor with two M36 threaded rod tie downs at each end to prevent rotation and shear keys were installed on both sides to prevent sliding. Horizontal loads were applied by a 400kN hydraulic actuator through a Ø50mm pin on the link beam. The loading point on the beam represents the point of contraflexture at the mid-span of a link beam. A pair of guide rails with nylon contact surfaces were installed on either side of the beam to restrain out-of-plane displacement (D_y) and twisting deformation about the beam's length (R_z).

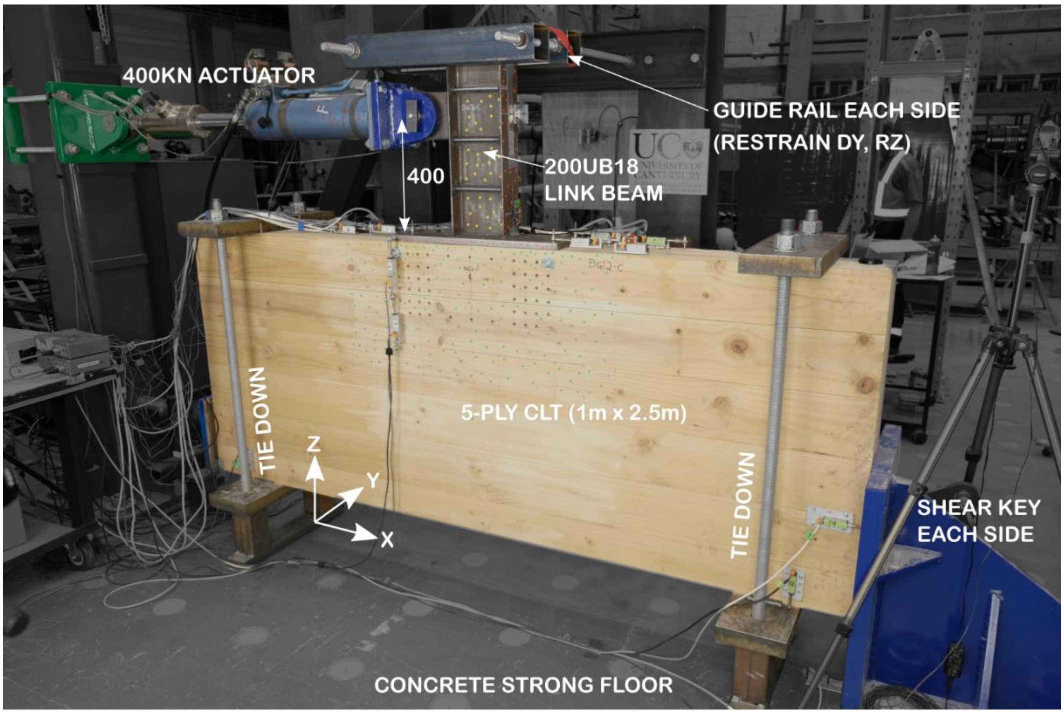

Figure 5: Experimental setup for cyclic testing of link beam specimens with SDD group connections.

The load was measured by a load cell on the hydraulic actuator and the displacement was measured by a string potentiometer. Rigid body movement of the CLT panel was monitored by spring potentiometers located at the shear key and at each tie down. Spring pots were also placed at the bases of the steel shear keys to measure lateral displacements. Additionally, two string potentiometers were connected to the beam flanges at the actuator height to monitor out-of-plane displacement and twisting of the link beam.

Local instrumentation in the connection region is shown in Figure 6. The lateral displacement of the connection was measured by horizontal linear potentiometers connected between the CLT edge and the steel end plate. The rotation of the connection was measured with a series of vertical potentiometers and calculated by fitting a linear trendline through the data points to determine the rotation. Strain gauges were also placed on the surface of the steel link beam.

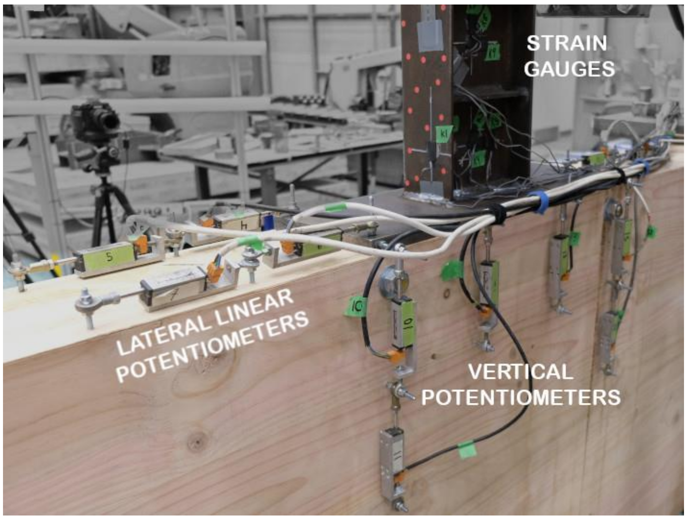

Figure 6: Local instrumentation for self-drilling dowel group connection specimen.

3.3. Displacement protocol

The monotonic test (DG10-M) was loaded at a constant load rate until adequate strength loss was achieved. The cyclic tests (DG11-C, DG12-C) used the displacement protocol from AISC 341 Section K2.4c [21]. This protocol is typically used to evaluate the performance of EBF link-to-column connections, an application similar to the connection in this study. According to the protocol, a series of increasingly large chord rotations are imposed while the number of cycle repetitions decreases as the rotation level increases, as shown in Figure 7. Displacement was applied at a rate between 5mm and 20mm per minute, increasing for the cycles with the largest chord rotations, but was held constant for each cycle. All tests were terminated upon reaching 50% strength loss from the peak strength.

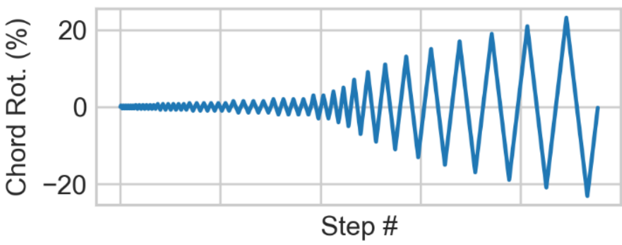

Figure 7: Loading protocol for cyclic link beam-to-wall connection tests.

4. Test Results and Discussion

Table 1 lists the key results including peak force (F_{pk}) and the corresponding moments in the beam ($M_{b,pk}$) and at the centroid of the dowel group ($M_{con,pk}$). The beam and connection moments are found by multiplying the force by the lever arm from the loading point to the end of the beam (380mm) and centroid of the connection (540mm), respectively. The distance from the loading point to the centroid of the SDD group was 540mm in the undeformed position but was adjusted to account for the loading pin moving along an arc path. The yield force and corresponding chord rotation (F_y, θ_y) were determined based on the intersection of two lines fit to the test data before and after the apparent yield point. Chord rotation was chosen as the deformation unit because it is a convenient design quantity used in coupled reinforced concrete wall design [25]. The lateral and rotational connection stiffnesses (k_v, k_m) were determined by fitting tangent lines in the range of 20% to 60% of F_{pk} on the backbone plots. The results of the cyclic tests include the values for the positive and negative cycles.

Table 1: Summary of observed peak forces, chord rotations, and connection stiffnesses.

ID	F_y	F_{pk}	$M_{b,pk}$	$M_{con,pk}$	θ_y	θ_{pk}	k_v	k_m
	kN	kN	kNm	kNm	rad	rad	kN/mm	kNm/rad
DG10-M	168	219	83	122	2.98%	11.8%	129	15,800
DG11-C	177/-178	250	95	124	2.83% / -2.89%	5.7% / -8.0%	153/-164	13800/-19300
DG12-C	178/-177	247	94	123	3.32% / -2.81%	8.4% / -8.1%	156/-134	12900/-13100

The cyclic peak loads were slightly higher than the monotonic peak load, as listed in Table 1. However, the cyclic specimens reached their peak strength at a lower displacement level. The beam's actual overstrength was reasonably close to the value calculated for capacity design, as shown by the dashed line in Figure 8b (250kN vs. 237kN). Therefore, the overstrength factor of 1.67 from NZS3404 [19] was appropriate.

4.1. Global behaviour and damage

The plotted test results are shown in Figure 8 with actuator force on the Y axis and chord rotation on the X axis. The chord rotation at each point is determined by dividing the actuator displacement (minus support sliding and rotation) by the distance from the loading point to the end of the I-beam (380mm). The link beam demonstrated a ductile failure and dissipated significant amounts of energy, as shown by the large hysteretic loops in Figure 8b. The cyclic tests showed a reduced deformation capacity and more strength loss when compared to the monotonic test due to accumulation of damage in the system through repeated cycles. The hysteretic behaviour of the cyclic tests closely resembles the results of long EBF link tests by Engelhardt and Popov [18]. It should be noted that the hysteretic behaviour in Figure 8b shows minor slips when the force in the system changed from unloading to loading due to some damage in the SDD group.

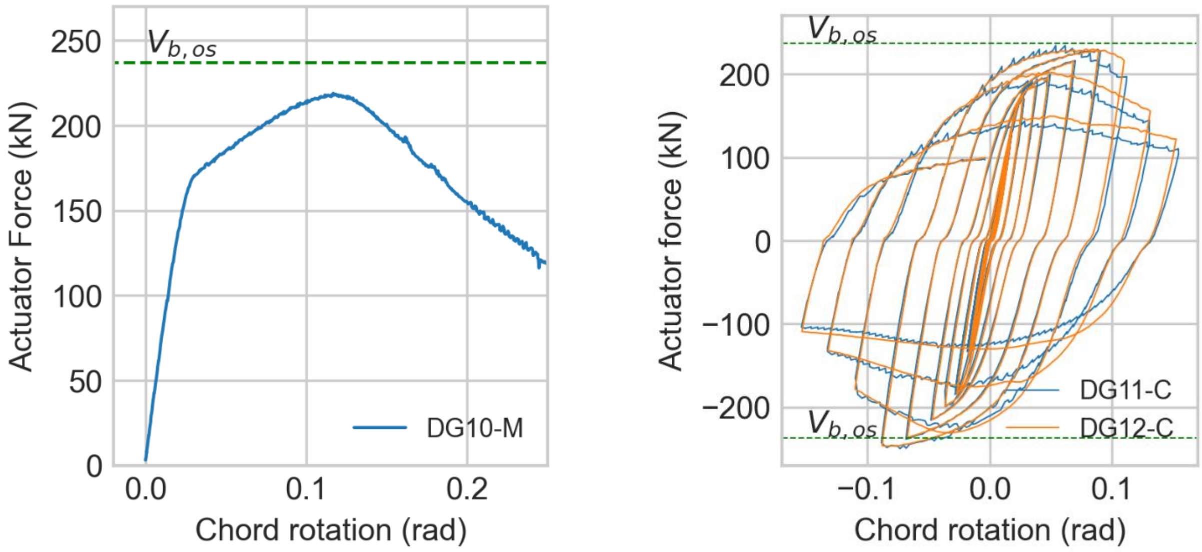

(a) (b)

Figure 8: Global force vs. chord rotation behaviour of monotonic (a) and cyclic tests (b).

Figure 9 shows the typical damage observed in each specimen. The link beam's lowest panel zone experienced web and flange yielding and inelastic buckling. Finally, the beam fractured at the web-flange joint (Figure 9b) which caused significant strength loss and led to the termination of the test. Although the damage in the connection is evident from the connection behaviour plots (Figure 10), the dowels were not measurably bent after disassembling the specimens. However, minor local crushing damage was observed around the dowel holes inside the CLT (Figure 9c).

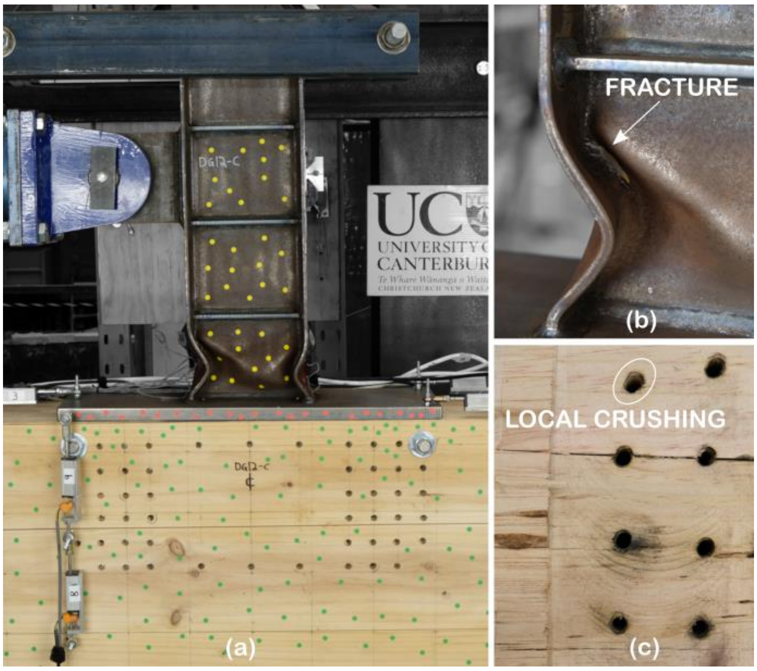

Figure 9: Observed damage including: (a) inelastic yielding and buckling of lowest panel zone in link beam, (b) fracture at flange-to-web joint, and (c) local internal crushing around the self-drilling dowel.

4.2. Connection behaviour

The connection behaviour is displayed in the plots of Figure 10. Plots a/b show the connection lateral behaviour, c/d show the rotational behaviour, and e/f show the normalized neutral axis depth (neutral axis location divided by length of end plate) against the connection rotation. The lateral and rotational plots do not exhibit linear elastic behaviour although the connection slip and rotation were relatively small. The pinched hysteresis loops are a typical response for dowel-type fasteners subjected to lateral loads. Minor connection damage is in part due to the chosen design approach which used the ultimate connection strength, rather than yield strength, to satisfy the capacity design requirements (see Section 2.3). The ultimate strength assumes a fully plastic behaviour of the connection and therefore implicitly accepts dowel yielding to redistribute the forces.

The last two cycles in the moment-rotation plots (Figure 10d) appear to indicate post-peak strength loss in the connection. However, this is not representative of the physical reality of tested specimens but was rather a result of the instrumentation method and asymmetric damage of the link beam. When the link beam experienced asymmetric flange fracturing, the loading on the end plate became eccentric and applied a twisting moment about the length of end plate. However, there was insufficient deformation data captured by the specimen's instrumentation to adequately quantify the twisting behaviour. The final three cycles of the moment-rotation plot include this twisting deformation and therefore are erroneous as they do not represent real post-peak behaviour or strength loss in the connection. A greater degree of out-of-plane restraint, such as that provided by an adjacent floor diaphragm, to the CLT wall panel may prevent or delay the observed asymmetric flange failure mode.

Plots of the neutral axis depth (Figure 10e and f) reveal a convergence towards a depth of approximately 35% of the end plate length from the toe. This value is in good agreement with the calculated contact length of 28% determined when analysing the connection with the analytical method described in Section 2.12.3.

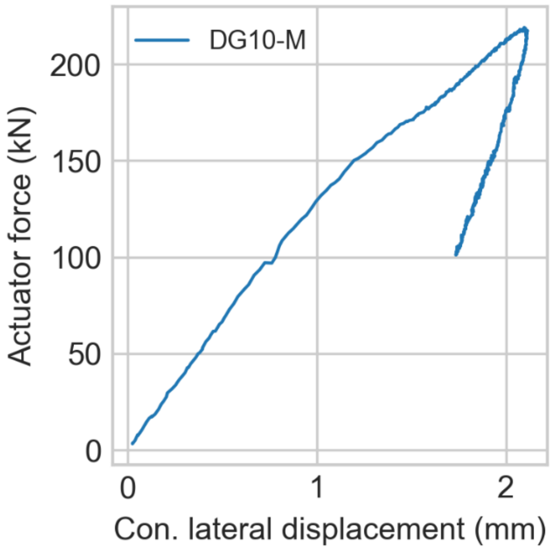
DG10-M
Actuator force (kN)
0
50
100
150
200
0
1
2
Con. lateral displacement (mm)

(a)

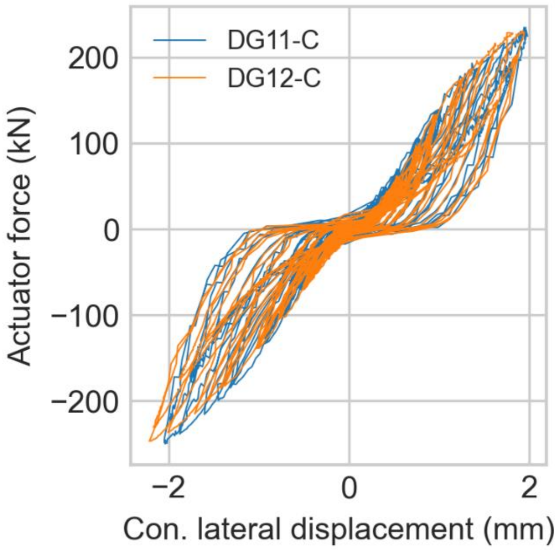
DG11-C
DG12-C
Actuator force (kN)
200
100
0
−100
−200
−2
0
2
Con. lateral displacement (mm)

(b)

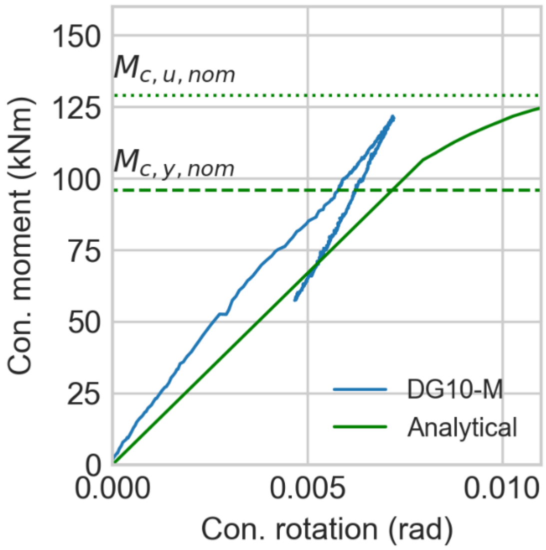
$M_{c,u,nom}$
$M_{c,y,nom}$
Con. moment (kNm)
0
25
50
75
100
125
150
DG10-M
Analytical
0.000
0.005
0.010
Con. rotation (rad)

(c)

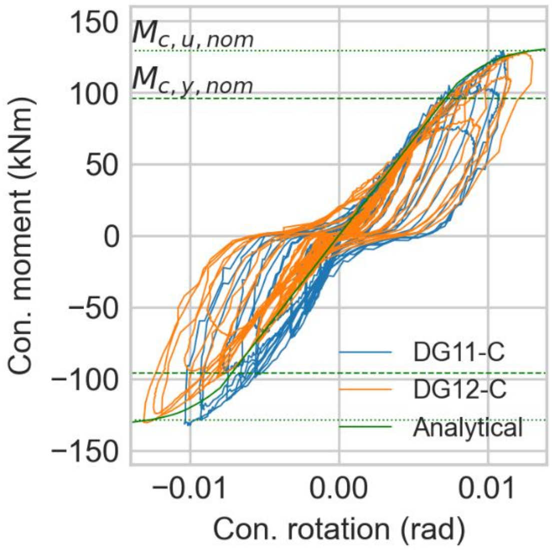
$M_{c,u,nom}$
$M_{c,y,nom}$
Con. moment (kNm)
150
100
50
0
−50
−100
−150
DG11-C
DG12-C
Analytical
−0.01
0.00
0.01
Con. rotation (rad)

(d)

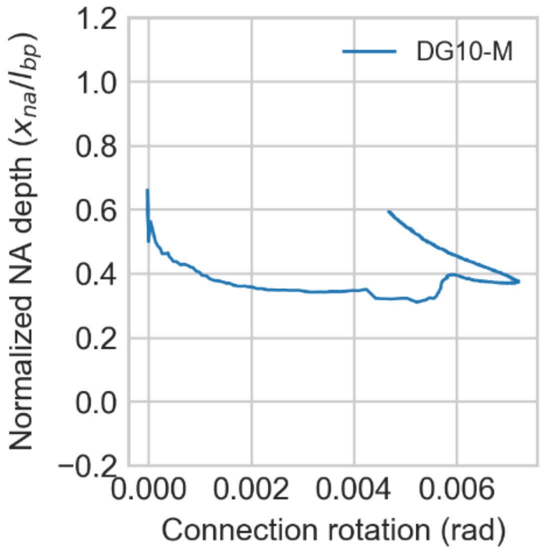

(e)

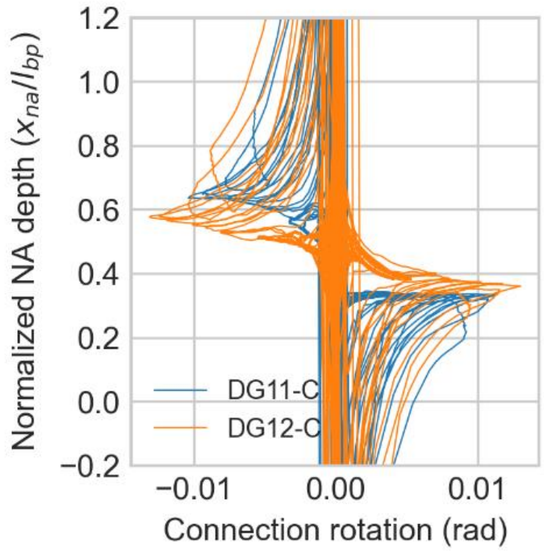

(f)

Figure 10: Monotonic and cyclic connection behaviour including: lateral (a,b), rotational (c,d), and normalized neutral axis depth (e,f).

Connection Stiffness

The mean connection stiffness values were 147 kN/mm and 15,000 kNm/rad for the lateral and rotational components, respectively. Using the approximate stiffness methods described previously in Section 2.2 with a mean density of 460kg/m^3, values of 160 kN/mm and 15,200kNm/rad are found. Both stiffness values were predicted reasonably well with errors of -9.4% and +1.2%, respectively. This level of error is likely acceptable for design purposes.

The moment-rotation backbone was predicted for the progressive yielding of the connection at the mean level with a typical SDD strength of F_d=11.2kN (f_h=35Mpa per Uibel and Blaβ [22]) and board compression strength of $f_{c,0}$=30Mpa (MSG8 axial test data [26] from Scion, a NZ research institute). The comparison agreed well with the backbones of the cyclic results shown in Figure 10d and 10e but under-predicted the monotonic response of DG10-M. This may be due to the cyclic loading causing progressive stiffness degradation which create better agreement with the predicted backbone.

The connection's lateral and rotational behaviour represent a significant source of deformation for the link beam and connection assembly. Table 2 shows the chord rotations for each specimen at the yield (θ_y) and peak (θ_{pk}) force levels with corresponding contributions from the lateral ($\theta_{y,cv}$, $\theta_{pk,cv}$) and rotational ($\theta_{y,cr}$, $\theta_{pk,cr}$) connection deformations. On average, the specimens reached their yield strength at a chord rotation of 2.97% radians including a connection chord rotation contribution of 0.99% radians (0.34% from lateral and 0.65% from rotational movement). A greater amount of chord rotation was observed in the connection components at the peak load but they were smaller relative to the total mean peak chord rotation of 8.39%. Additional in-plane CLT deformations further contribute to the flexibility of the system but were not specifically captured by the specimen's instrumentation.

Table 2: System and connection chord rotations observed at yield and peak forces.

Specimen	θ_y	$\theta_{y,cv}$	$\theta_{y,cr}$	θ_{pk}	$\theta_{pk,cv}$	$\theta_{pk,cr}$
DG10-M	2.98%	0.38%	0.56%	11.8%	0.55%	0.72%
DG11-C	2.83% / -2.89%	0.33% / 0.32%	0.67% / 0.51%	5.7% / -8.0%	0.51% / 0.54%	1.09% / 1.02%
DG12-C	3.32% / -2.81%	0.34% / 0.35%	0.75% / 0.76%	8.4% / -8.1%	0.51% / 0.58%	1.23% / 1.29%
mean	2.97%	0.34%	0.65%	8.39%	0.54%	1.07%

The connection's flexibility increases the chord rotation required to reach the yield strength of the link beam. Considering a 200UB18 cantilever beam with L=380mm and F_y=300MPa, a predicted yield chord rotation can be calculated as 0.50% using basic beam theory as $P/GA_w + PL^2/3EI_{xx}$ where P is equal to the observed yield strength of the beam (170kN). This predicted chord rotation is approximately 1/6th of the actual chord rotation observed in the experiments and represents an estimate of the chord rotation contribution of the steel beam element. As discussed above, 0.99% out of the 2.97% chord rotation was attributed to the connection. Therefore, an approximate mean chord rotation of 1.5% (2.97% - 0.50% - 0.99%) can be attributed to the in-plane deformations of the CLT panel.

Therefore, it is critical to consider the connection stiffness and in-plane CLT deformations in the analysis of a coupled wall system as they significantly affect the deformations at which the link beams yield and dissipate energy. However, the in-plane CLT deformations will change based on the width and thickness of the CLT in a coupled wall structure.

Initial Displacement

The initial displacement of the SDD connection was minimal due to the nature of the self-drilling dowel but it was not exactly zero and increased with repeated cyclic loading. This can be observed in the cyclic lateral and rotational connection plots (Figure 10b and d). Residual displacements and pinching behaviour developed after repeated cycles and can be observed in the region where the specimen changes from unloading to loading and crosses the X axis. This residual displacement and sudden stiffness decrease caused the pinched shape in the connection hysteresis.

4.3. Energy dissipation

The energy dissipated by the specimen, shown in Figure 11 with the initial cycles truncated, was dominated by yielding of the steel link beam. The dissipated energy in the connection is also shown for the lateral (v) and rotational (r) degrees of freedom. The connection contributions represent a small portion of the total dissipated energy in the system and their magnitude relative to the total dissipated energy reaches a plateau as the chord rotation increases.

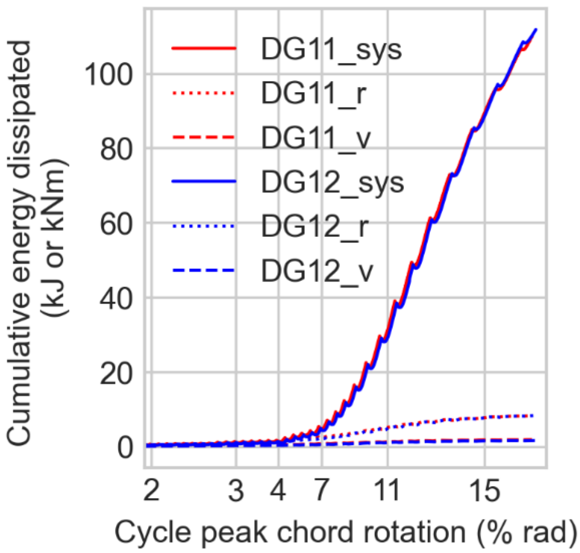

Figure 11: Cumulative energy dissipation of cyclic tests for the global system and connection behaviour.

5. Conclusions

Coupled CLT shear walls with steel link beams have a great potential to be used in mass timber buildings since they provide a more structurally efficient lateral load resisting system compared with single cantilever shear walls. The connections between the steel link beams and the CLT wall panels are critical to the efficiency and robustness of the coupled wall system. This study presented one possible connection solution using a group of SDDs for 200UB18 link beams in a 5-ply CLT wall. Based on this work, the following conclusions are made:

1. The SDD groups in this study were successfully capacity-protected for the overstrength of dissipative 200UB18 link beam elements.
2. The ultimate (rather than yield) strength of the SDD group connection can be used to satisfy the capacity design requirements with minor damage occurring due to timber embedment crushing. This may be acceptable depending on the performance requirements selected by the designer.
3. The presented analytical methods for determining the strength and stiffness of the SDD connections provided reasonable estimations when compared with the test results.
4. The connection stiffness and in-plane CLT deformations significantly increase the chord rotation required to yield the link beam elements. Therefore, they must be carefully considered in the system-level analysis.

This study was limited to the analysis and testing of three full-scale specimens which were capacity designed to facilitate yielding of the steel link beams. Future work may include the consideration of axial loads in the link beams, different connection details, CLT layups, or steel link beam sections.

Acknowledgements

This research was funded by the WIDE Trust, SWP Research Partnership, and Earthquake Commission Biennial Grants in New Zealand. The authors are grateful for their support and for the technical support in the laboratory from Alan Thirlwell, David Carney, and Michael Weavers.

References

[1] M. Green, The Case for Tall Wood, Second Edition, 2017.

[2] X. Zhang, Seismic Design of Timber Steel Hybrid High-Rise Buildings, Doctor of Philosophy, University of British Columbia, 2017.

[3] X. Zhang, M. Fairhurst, T. Tannert, Ductility Estimation for a Novel Timber–Steel Hybrid System, J. Struct. Eng. 142 (2016). https://doi.org/10.1061/(ASCE)ST.1943-541X.0001296.

[4] X. Zhang, M. Shahnewaz, T. Tannert, Seismic reliability analysis of a timber steel hybrid system, Engineering Structures. 167 (2018) 629–638. https://doi.org/10.1016/j.engstruct.2018.04.051.

[5] P. Bhat, Experimental Investigation of Connection for the FFTT, A Timber-Steel Hybrid System, Master’s Thesis, University of British Columbia, 2013.

[6] M.R. Azim, Numerical and experimental investigations of connection for timber-steel hybrid system, Master’s Thesis, University of British Columbia, 2014.

[7] X. Zhang, M.R. Azim, P. Bhat, M. Popovski, T. Tannert, Seismic performance of embedded steel beam connection in cross-laminated timber panels for tall-wood hybrid system, Can. J. Civ. Eng. 44 (2017). https://doi.org/10.1139/cjce-2016-0386.

[8] WPMA, NZ Wood Design Guide - Portal Knee Connections, (2020).

[9] R.J. Bainbridge, C.J. Mettem, A review of moment-resistant structural timber connections, Proceedings of the Institution of Civil Engineers - Structures and Buildings. 128 (1998). https://doi.org/10.1680/istbu.1998.30909.

[10] F. Lam, M. Gehloff, M. Closen, Moment-resisting bolted timber connections, Proceedings of the Institution of Civil Engineers - Structures and Buildings. 163 (2010). https://doi.org/10.1680/stbu.2010.163.4.267.

[11] W. Dong, M. Li, M. He, Z. Li, Experimental testing and analytical modelling of glulam moment connections with self-drilling dowels, Journal of Structural Engineering. (2021). https://doi.org/10.1061/(ASCE)ST.1943-541X.0002977.

[12] A. Ringhofer, R. Brandner, H.J. Blaß, Cross laminated timber (CLT): Design approaches for dowel-type fasteners and connections, Engineering Structures. 171 (2018) 849–861. https://doi.org/10.1016/j.engstruct.2018.05.032.

[13] K.W. Johansen, Theory of timber connections, International Association of Bridge and Structural Engineering, Bern, Switzerland, 1949.

[14] H.J. Blaß, C. Sandhaas, Timber Engineering - Principles for design, KIT Scientific Publishing, Karlsruhe, Germany, 2017.

[15] European committee for Standardization (CEN), Eurocode 5. Design of timber structures - Part 1-1: General - Common rules and rules for buildings., (2003).

[16] R. Park, T. Paulay, Reinforced concrete structures, Wiley, New York, NY, 1975.

[17] M.N. Fardis, Capacity design: Early history, Earthquake Engng Struct Dyn. 47 (2018). https://doi.org/10.1002/eqe.3110.

[18] M.D. Engelhardt, E.P. Popov, Experimental Performance of Long Links in Eccentrically Braced Frames, Journal of Structural Engineering. 118 (1992). https://doi.org/10.1061/(ASCE)0733-9445(1992)118:11(3067).

[19] New Zealand Standard, NZS3404:1997 Steel structures standard (Incorporating Ammendments 1 and 2), (2007).

[20] Australia/New Zealand Standard, AS/NZS 3679.1:2016 Structural Steel - Part 1: Hot-rolled bars and sections, (2016).
[21] AISC, ANSI/AISC 341-16 Seismic Provisions for Structural Steel Buildings, (2016).
[22] Thomas Uibel, Hans J Blaß, Load Carrying Capacity of Joints with Dowel Type Fasteners in Solid Wood Panels, in: Proc. CIB W18 Meeting 39, Florence, Italy, 2006.
[23] Rothoblaas, Self-perforating dowel | WS | Rothoblaas, (2021). https://www.rothoblaas.com/products/fastening/screws/screws-structures/ws (accessed January 29, 2021).
[24] New Zealand Standard, NZS 3603:1993 Timber Structures Standard, (2005).
[25] T. Paulay, The displacement capacity of reinforced concrete coupled walls, Engineering Structures. 24 (2002). https://doi.org/10.1016/S0141-0296(02)00050-0.
[26] D. Gaunt, MSG - Strength and Stiffness Distributions, Scion, Rotorua, NZ, 2006.